FINITE ELEMENT IMPLEMENTATION OF A MODEL FOR LONGITUDINAL COMPRESSIVE DAMAGE GROWTH WITH FRICTION

Sérgio Costa[1,2], Renaud Gutkin[1] and Robin Olsson[1]

[1]Swerea SICOMP AB, SE-431 22, Mölndal, Sweden
[2]Department of Applied Mechanics, Chalmers University of Technology, 412 96 Gothenburg, Sweden
Email: sergio.costa@swerea.se, renaud.gutkin@swerea.se, robin.olsson@swerea.se
Web Page: http://www.swerea.se/sicomp

Keywords: Crushing, kinking, friction, damage mechanics, FEA

Abstract
A model for the longitudinal response of laminated fibre-reinforced composites during compressive damage growth is implemented in a Finite Element (FE) package and validated for mesh objectivity. The current work details the FE implementation of the fibre kinking model and in particular challenges associated with mesh objectivity. The numerical way to solve the stress equilibrium and stress compatibility equations simultaneously in an FE framework is also presented. The results show that the current model can be used to predict the kinking response and thus account for the correct energy absorption.

1. Introduction

From all intralaminar failure modes, the one that has been most referred in the literature is kink band formation or simply kinking. The interest in this particular failure mode is mainly due to the need to orient fibres at zero degrees in designs for stiffness, strength and energy absorption. There are well established models to predict stiffness and strength but not for energy absorption, i.e. the post-peak response is not correctly addressed. Kinking is a very complex phenomenon due to the interacting mechanisms and due to the instability created at failure. The representative models in the literature are mainly analytical and FE models based on micromechanics [1-3]. However, none of the approaches is able to represent the behaviour of large and complex structures in multiaxial loading situations.

The proposed model is based on Continuum Damage Mechanics (CDM) and it homogenizes the fibres and the matrix together at the ply level (mesoscale), thus less computationally expensive and suitable for larger structures. In spite of the general belief, fibre kinking is considered a matrix dominated failure mode [4] and an accurate matrix response becomes necessary to predict the kinking response. Thus the transverse and the shear responses used in the present model are based on a physical coupling between damage growth and friction created at microcrack closure as described in [5]. As a result a non-zero frictional stress acts on crack faces when the material is partially or fully damaged. This type of modelling is important to account for the correct energy dissipation at different strain levels, e.g. during progressive crushing in car crash situations.

The longitudinal response is obtained by using fibre kinking theory, Fleck et al. [2], i.e. non-perfectly straight fibres rotating under an applied compressive load induce a loss of stability in the resin that eventually leads to kink-band formation. This framework is extended to predict the response after the

Excerpt from ISBN 978-3-00-053387-7

peak load. The current model is able to predict the whole kinking response under a 3D stress state. The peak stress results from shear instability due to the highly nonlinear shear response [6]. The resulting compressive-softening behaviour differs greatly from the most commonly used bilinear approaches.

2. Overview of the constitutive model

The fibre kinking response is found from solving simultaneously (i) the stress equilibrium between applied global stresses and nonlinear local stresses resulting from (ii) the nonlinear constitutive law of the material in the kink-band. The actual rotation of the fibres in the kink-band is resolved from (iii) the strain compatibility, as detailed in [3]. In summary the kink-band is influenced by the compressive longitudinal strains, the transverse and the shear stresses as well as the misalignment of the fibres in the composite.

2.1. Geometrical perspective

The kinking phenomenon has a strong 3D nature which requires a 3D framework for an accurate prediction. The development of the current 3D model is explained in detail in [3]. The FE implementation is detailed here as well as a succinct summary of the model.

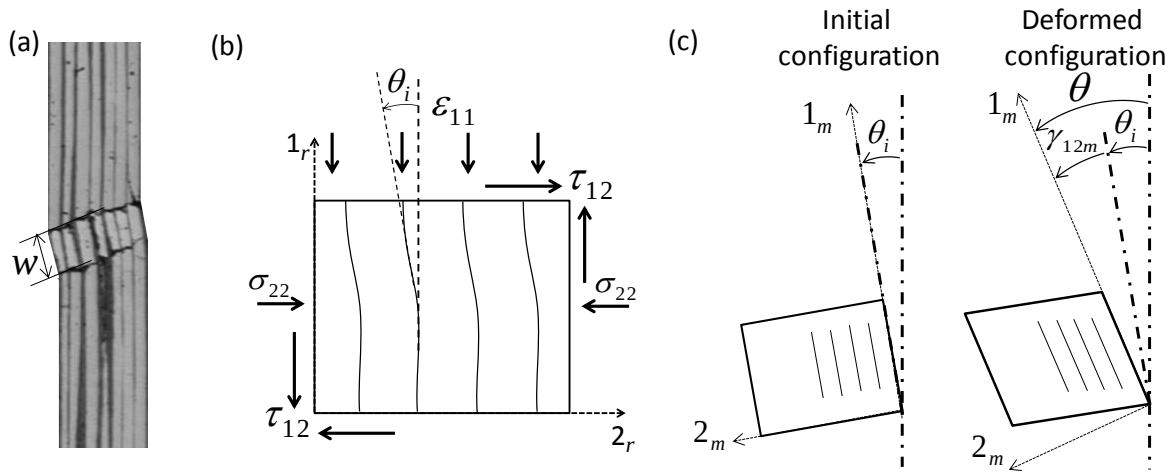

Figure 1. Illustration of the present kinking model

Figure 1(a) shows a micrograph of a typical kink-band. Two coordinate systems are introduced: the first one rotated to the orientation of the kink-band through the thickness is denoted *r* and the second (misaligned) coordinate system, *m*, is associated with the rotating fibres and is characterised by the angle θ. The factors contributing to fibre rotation in the kink-band are represented in Figure 1(b). Figure 1 (c) defines the initial and current configurations and associated fibre rotations. The numerical subscripts (11, 22, 12) refer to the global coordinate system and the subscripts using *m* (11*m*, 22*m*, 12*m*) refer to the misaligned frame, ***m*,** also referred to as local frame or kink band frame later on.

Based on Figure 1(c) the following relation can be established

$$\theta = \gamma_{12m} + \theta_i \tag{1}$$

Excerpt from ISBN 978-3-00-053387-7

2.2. Model formulation

The current model predicts the longitudinal compressive response for an arbitrary loading. The three conditions aforementioned, (i) to (iii) are summarized in the equations that follow. Starting with strain compatibility (iii), which can be expressed as a function of the shear angle as

$$f(\gamma_{12m}) = \varepsilon_{11m}c^2 + \varepsilon_{22m}s^2 - \gamma_{12m}cs - \varepsilon_{11} = 0 \tag{2}$$

where $c = \cos(\theta)$ and $s = \sin(\theta)$. Using numerical methods it is possible to find a γ_{12m} which satisfies Equation (2). For the remaining unknowns one can take advantage of the elastic assumptions. Thus, the strains in the kink band coordinate system can be expressed as

$$\varepsilon_{11m} = \frac{\sigma_{11m}}{E_{11}} - \frac{\nu_{12}}{E_{11}}\sigma_{22m} \qquad \varepsilon_{22m} = \frac{\sigma_{22m}}{E_{22}} - \frac{\nu_{12}}{E_{11}}\sigma_{11m} \tag{3}$$

To solve the previous set of equations it becomes necessary to establish the stress equilibrium (i), which will constitute the second set of equations as follows:

$$\begin{pmatrix} \sigma_{11m} \\ \sigma_{22m} \\ \tau_{12m} \end{pmatrix} = \begin{bmatrix} c^2 & s^2 & 2sc \\ s^2 & c^2 & -2sc \\ -sc & sc & c^2 - s^2 \end{bmatrix} \begin{pmatrix} \sigma_{11} \\ \sigma_{22} \\ \tau_{12} \end{pmatrix} \tag{4}$$

where the stresses on the Right Hand Side (RHS) are in the *r* coordinate frame. The stress component of interest is the kinking stress, σ_{11}. However, the transverse and the shear stresses need to be calculated from (ii) which constitutes the nonlinear response of the matrix. The shear response accounts for nonlinearity by combining damage with friction in a physical way according to [5] as follows

$$\tau_{12m} = G_{12}\gamma_{12m}(1-d) + d\tau^{friction} \tag{5}$$

where $\tau^{friction}$ represents the in-plane frictional stress and *d* is the state of damage detailed in [3]. Finally, from the third row in Equation (4) the kinking stress is given by

$$\sigma_{11} = \left[\sigma_{22}sc + \tau_{12}(c^2 - s^2) - \tau_{12m}\right]/(sc) \tag{6}$$

2.2.1 *Simplification of the model*

Only for a more tangible understanding the previous equation can be simplified assuming uniaxial stress state (σ_{22}=τ_{12}=0) and small rotations. It results in a variant of Budiansky's equation [4] in which the shear and compressive strengths are replaced by the in-plane shear and kinking stresses respectively

$$\sigma_{11} = \frac{-\tau_{12m}}{\gamma_{12m} + \theta_i} \tag{7}$$

From the simplification above it becomes clearer that fibre kinking is driven by matrix failure and strongly influenced by the initial fibre misalignment. Many authors have identified θ_i as the variable that incorporates the defects (voids etc).

2.3. Material properties

The material data used in this manuscript was taken from [7] which provides further information about the characterisation of the mechanical properties. The parameters necessary for the model were gathered in Table 1. The in-plane shear strength, S_L, is the value at the *onset* of shear nonlinearity. The parameter p_{0L} accounts for the internal pressure in the longitudinal direction built up during manufacturing. The kink band width, *w*, Figure (1a), was assumed to be 0.2 mm just for convergence studies.

Excerpt from ISBN 978-3-00-053387-7

Table 1. Mechanical properties of the uni-weave NCF composite HTS45/LY556

Elastic properties				
Modulus (GPa)			Poisson's ratios	
$E_{11}=136$	$E_{22}=9.15$	$G_{12}=4.9$	$\nu_{12}=0.28$	$\nu_{23}=0.43$
Strength properties (MPa)			**Kinking parameters**	
$X_t=1787$	$Y_t=29$	$S_L=20$	$p=-0.7$	w = 0.2 mm
$X_c=626$	$Y_c=130$	$S_T=47.44$		
Friction properties				
Internal pressure (MPa)			Coefficient of friction	
$p_{0L}=60$	$p_{0T}=30$		$\mu_L=0.34$	$\mu_T=0.4$

2.4. Results at the material point

The stress-strain relation predicted by the current model can be partially validated by two test cases. In the first case, the peak stress and corresponding strain during uniform axial loading, as reported in [7], is correlated with stresses and strains at failure, indicated by crosses in Figure 2. It is evident that the results are in good agreement with the model predictions for typical misalignment angles of 2.5° to 3.5°. The scatter in results reflects the strong influence of initial fibre misalignment angles. In the second case the predicted stress for large compressive strains is in good agreement with the measured average crush stress [8], as indicated in Figure 2.

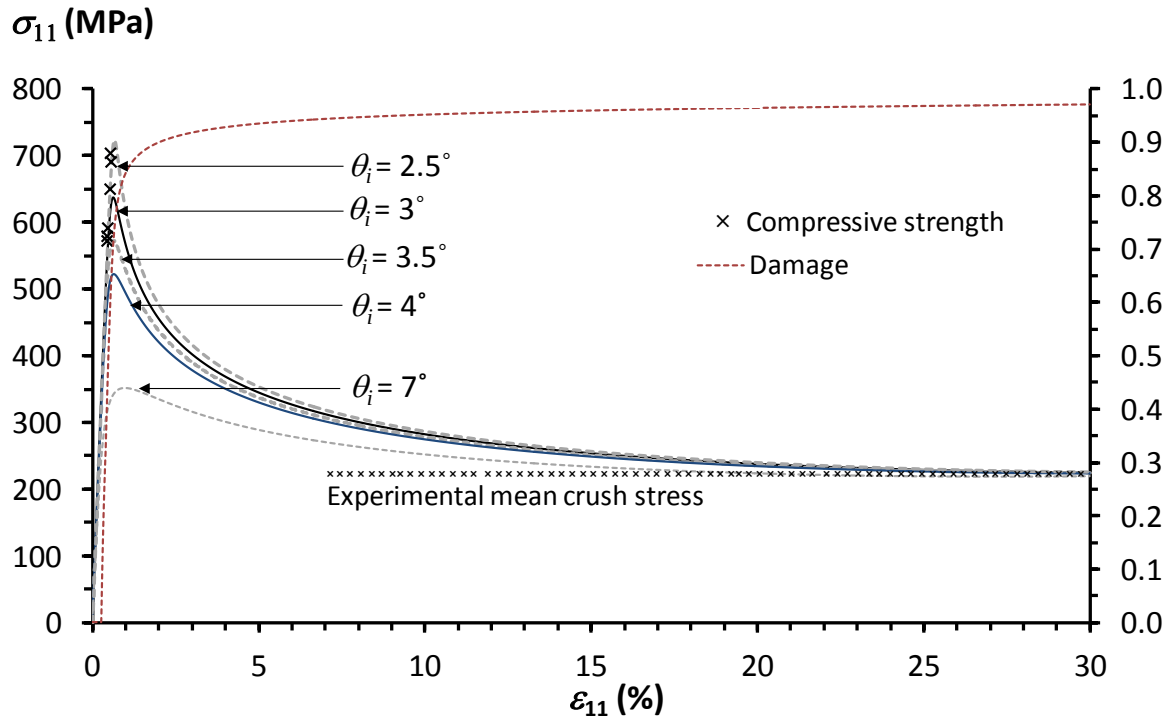

Figure 2. Model response for fibre compression for different fibre misalignments vs. experiments: Strength and mean crush stress

Excerpt from ISBN 978-3-00-053387-7

3. FE implementation

The model described previously was implemented into a user subroutine, VUMAT, in the commercial FE code ABAQUS. The main numerical challenges are related to the solution of Equation (4) and (5) and to the mesh objectivity due to the softening behaviour.

Damage growth is the main dissipative mechanism in CFRP. This is modelled through a damage variable, d, and the effect of damage degrades stress components and regulates the friction contribution. The damage must assume values between 0 (no damage) to 1 (fully damaged material), giving the following equation for the current damage variable at a given increment n:

$$d^n = \max\left\{0, \min\left\{d^n, 1\right\}\right\} \tag{8}$$

Damage is irreversible, i.e. the damage effects cannot be recovered. This condition is the assumption for unloading; following that the damage variable is redefined as

$$d^n = \max\left\{d^n, d^{n-1}\right\} \tag{9}$$

3.1. Solution procedure for Equations (1) to (6)

In order to solve the stress equilibrium and the strain compatibility it is necessary to use a root-finding method. In the current approach the bisection method was chosen. The reasons to choose this method over other methods with faster convergence are its simplicity and robustness, particularly close to the peak load. Taking advantage of the simplicity of bisection one can directly write all the equations as described into the model formulation. Using methods with faster convergence will require coupling Equations (1-6) into two equations, to solve for two unknowns, in order to calculate their respective derivatives (either analytically or numerically). In the following analyses we will consider the case with $\theta_i = 4°$.

3.2. Mesh objectivity

The challenge with damage models is that they have a softening response, which makes it necessary to deal with the strain softening behaviour. A cube of side L=1 mm was meshed with one element (1x1x1) and successively refined till (5x5x5). When more elements are added, the softening response is mesh dependent, Figure 3.

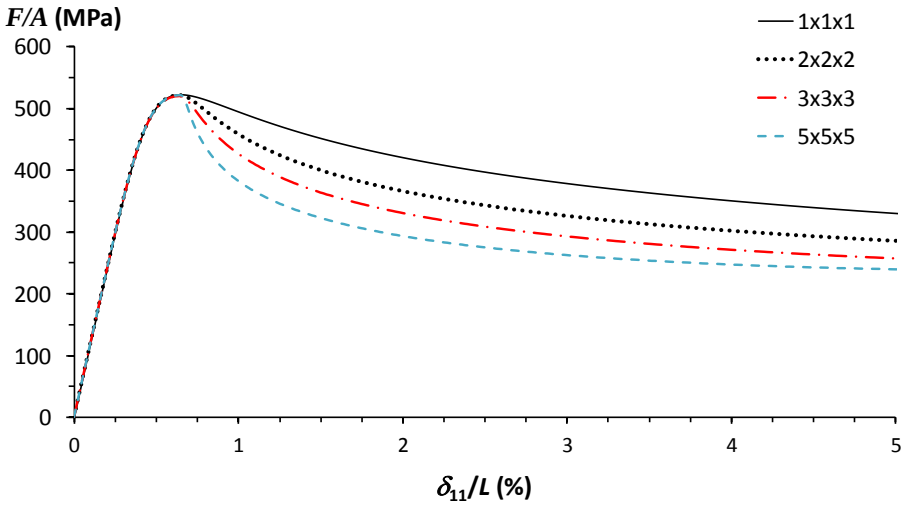

Figure 3. FE model responses showing the mesh dependency issue

Excerpt from ISBN 978-3-00-053387-7

In order to solve the mesh objectivity issues, previous models [6] took advantage of the critical strain energy release rate G_c to define the final strain (for the fully damaged material) that is proportional to the element characteristic length. However, in the current model, G_c is not used, which is a major advantage for model simplicity but an extra difficulty for FE implementation. Thus, one possible approach is to scale the strain with the kink-band width (w), which is a material parameter.

3.2.1 *Method 1 – Strain decomposition*

As shown in Figure 4, Method 1 decomposes the strain into a bulk/elastic component ε_{el}, and a kink band component ε_k. The total displacement, δ is expressed as

$$\delta = \delta_k + \delta_{el} \Rightarrow \bar{\varepsilon} L_e = \varepsilon_k w + \varepsilon_{el}(L_e - w) \tag{10}$$

where $\bar{\varepsilon}$ is the total strain applied to the element. The previous equation can be rearranged and the kinking strain becomes

$$\varepsilon_k = \left[\bar{\varepsilon} - (1-\overline{w})\sigma_{11}/E_{11}\right]/\overline{w}\text{, where } \overline{w} = w/L_e \tag{11}$$

where the kinking stress, σ_{11} must be recovered from a previous iteration. The whole iteration process stops when the tolerance criterion is met. These iterations add computational costs. Another important drawback with this method is the snap-back behaviour observed for ratios of $\overline{w}$ smaller than one-fourth, oberved in Figure 4 for 1 element. The results are shown in Figure 4(a) and the elements with higher damage are shown in red (or lighter colour) in Figure 4(b). The solution "5x5x5, no method" corresponds to the case when the element size coincides with the kink band width, i.e. $\overline{w}$ =1, which allows simulation of the kink band localisation in the real material. The agreement with the other curves confirms the mesh objectivity.

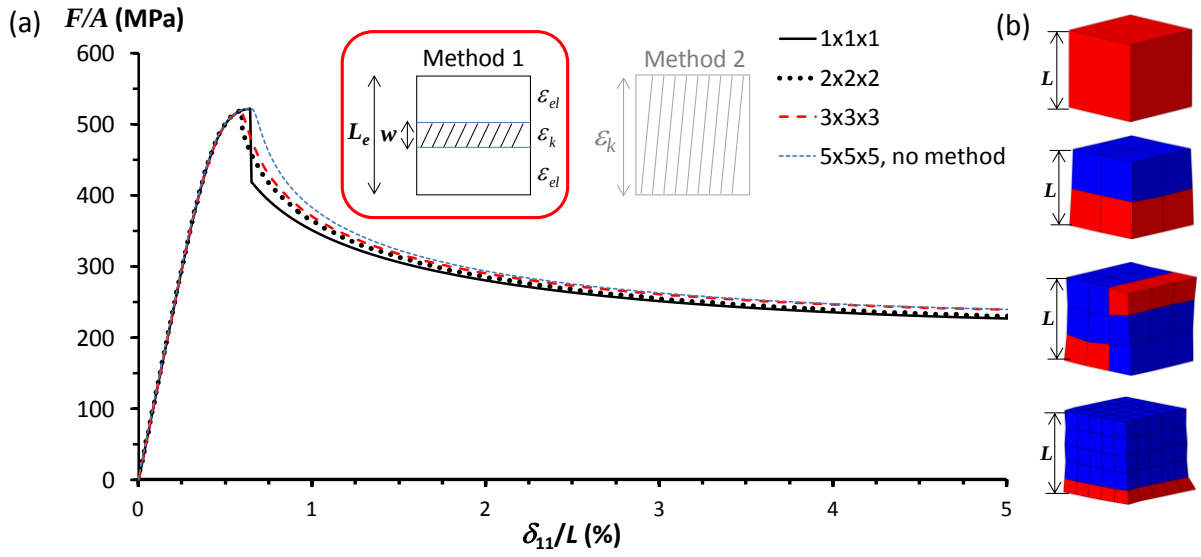

Figure 4. Method 1: (a) kinking responses, (b) respective mesh refinements

3.2.2 *Method 2 – Smear the kink-band over the element*

In this method the strain in the kink-band is distributed (smeared) over the whole element. The strain at the peak stress is denoted ε_o, Figure 5(a) Thus, when softening starts, i.e. when the peak stress has been reached, the kinking strain is split using the following strain-decomposition

$$\varepsilon_k = \varepsilon_o + \varepsilon_{soft} \Rightarrow \varepsilon_k = \varepsilon_o + \left(\bar{\varepsilon} - \varepsilon_o\right)L_e / w \tag{12}$$

This method is computationally cheaper and more stable when compared to method 1, since there is no need to iterate on the kinking stresses again.

Excerpt from ISBN 978-3-00-053387-7

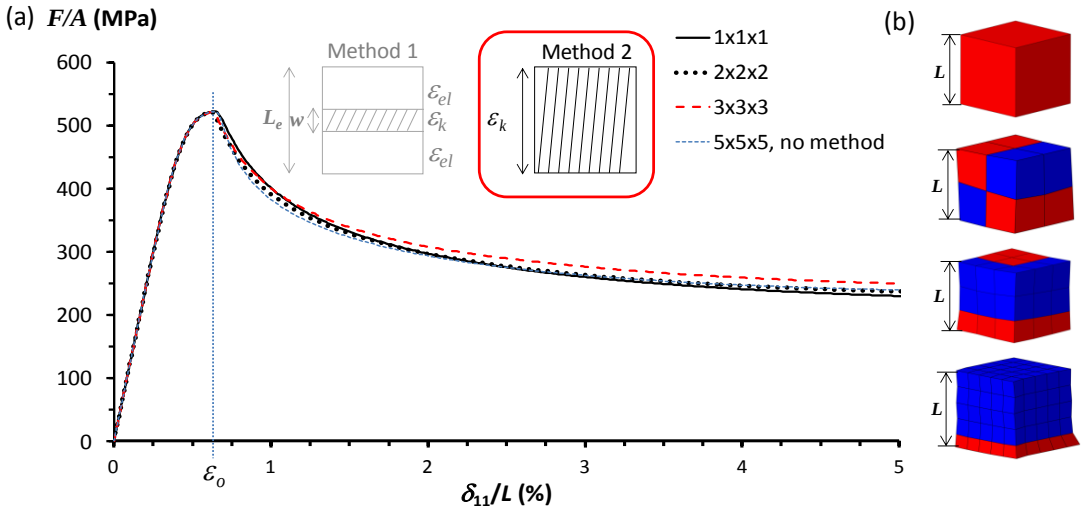

Figure 5. Method 2: (a) kinking responses, (b) respective mesh refinements

3.3. Unloading effects

In a model with multiple elements some of them undergo softening behaviour when the peak stress has been reached, i.e. the absolute value of the longitudinal strain, $|\varepsilon_{11}|$ decreases, representing an unloading situation. The unloading behaviour for two examples of unloading-loading cycles shown in Figure 6 is based on the sliding-sticking response of the friction, as described in [4]. The shear instability has been defined according to [6].

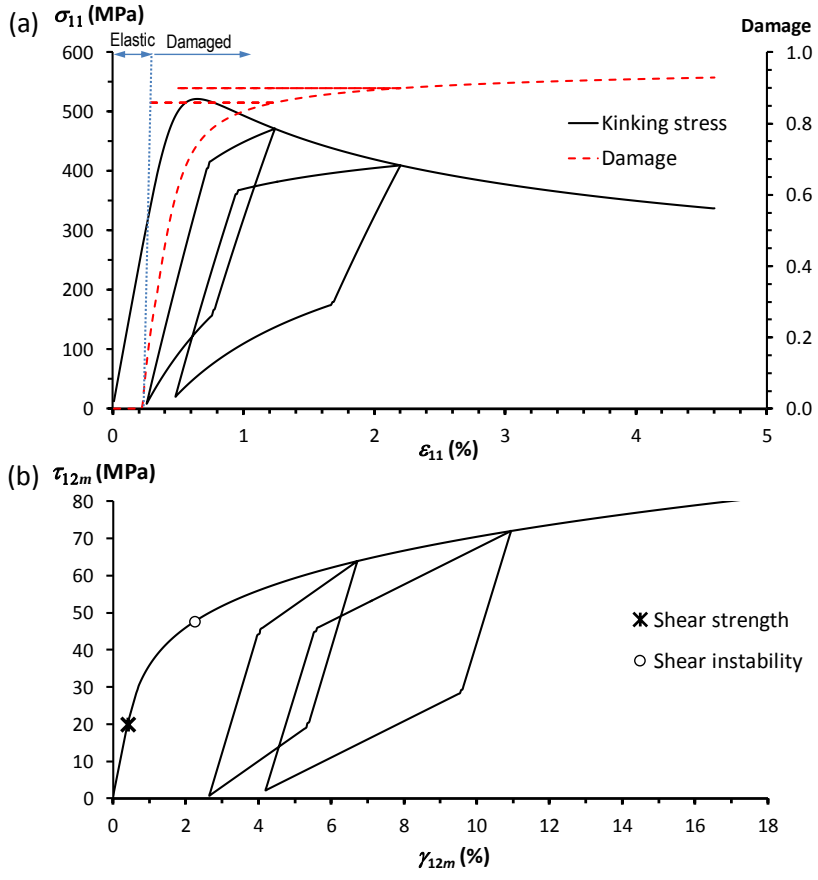

Figure 6. Cyclic response: (a) cyclic kinking stress and associated damage, (b) cyclic shear stress

Excerpt from ISBN 978-3-00-053387-7

During unloading the damage variable remains constant following Equation (9). The shear response for the model is shown in Figure 6 (b). The increase of the permanent strain from the first to the second loop is evident, which constitutes an asset of the model. The shear strength represented, S_L in Table 1 dictates the initiation of the damage variable. Shear instability occurs at higher shear strains, resulting in the inversion of the kinking response, i.e. the kinking strength is determined by shear instability.

4. Conclusions

An FE implementation of a validated material model is detailed with special attention to mesh objectivity. The bisection root finding method was used with satisfactory results for solving the stress-equilibrium and the strain-compatibility with robustness and simplicity. The mesh objectivity, a major issue with many models with softening behaviour, is resolved for different refinement levels. It is shown that a method based on strain decomposition gives mesh objective results but is limited in element size as elastic snap-back otherwise takes place. A smeared method removes this issue while preserving the mesh objectivity.

5. Future work

Since the implemented analytical model has proven to represent the experiments, the FE model should be able to do the same. Nevertheless, due to the complexity of crash, the current FE model needs to be validated against experimental data. Therefore, the interaction of fibre kinking with other failure mechanisms will be addressed in the continuation of the current work.

Acknowledgments

The funding for this research from Fordonsstrategisk Forskning och Innovation (FFI) via VINNOVA is gratefully acknowledged.

References

[1] S. Pimenta, R. Gutkin, S.T. Pinho and P. Robinson. A micromechanical model for kink-band formation: Part II—Analytical modelling. *Composites Science and Technology*, 69 (7-8), 956–964, 2009

[2] N.A. Fleck, L. Deng, B. Budiansky. Prediction of Kink Width in Compressed Fiber Composites. *Journal of Applied Mechanics*, 62(2), 329, 1995.

[3] R. Gutkin, S. Costa, R. Olsson, A physically based constitutive model for kink-band growth and longitudinal crushing of composites under 3D stress states. *Composites Science and Technology*, 2016, submitted

[4] B. Budiansky. Micromechanics. *Computers & Structures*, 16(1-4), 3–12, 1983.

[5] R. Gutkin and S.T. Pinho. Combining damage and friction to model compressive damage growth in fibre-reinforced composites. *Journal of Composite Materials*, 49, 2483–2495, 2015

[6] S.T. Pinho, L. Iannucci, P. Robinson. Physically based failure models and criteria for laminated fibre-reinforced composites with emphasis on fibre kinking. Part II: FE implementation. *Composites Part A: Applied Science and Manufacturing*, 37(5), 766– 777, 2006

[7] T. Bru, P. Hellström, R. Gutkin, D. Ramantani, G. Peterson. Characterisation of the mechanical properties of a uni-weave carbon fibre/epoxy non-crimp fabric composite. *Data in Brief*, 6, 680–695, 2016.

[8] T. Bru, P. Waldenström, R. Olsson, R. Gutkin and G. Vyas. Investigation of the longitudinal and transverse crushing behaviour of unidirectional flat specimens. *Composites Part A: Applied Science and Manufacturing*, 2016, submitted

Excerpt from ISBN 978-3-00-053387-7